

# Computer Simulation of Processes at Electron and Ion Beam Lithography, Part 1: Exposure Modeling at Electron and Ion Beam Lithography

Katia Vutova and Georgi Mladenov  
*Institute of electronics, Bulgarian Academy of Sciences  
Bulgaria*

## 1. Introduction

Increasing the electronic circuit density is a major trend in microelectronics. Lithography is the key technology for the fabrication of very large integrated circuits with smaller device sizes. Today conventional optical lithography is approaching its fundamental physical limits. Electron and ion lithographies are among various candidates capable of sub-150 nm resolution for the new generation of lithographic techniques. Nanometer scale device fabrication rules require tight control of the developed polymer resist profile. Process simulation is a key tool for optimization of the obtained lithography results.

The goal of the computer simulation of the processes at electron and ion beam lithography (EBL and IBL) is the resist profile prediction of developed patterns after exposure of samples, covered by a sensitive polymer resist layer, which is sensitive to irradiation by accelerated particles. The accuracy of the simulated resist profiles strongly depend on the physical knowledge of the processes as well as on the accuracy of the process parameters.

The main step of such modeling: (i) exposure process modeling (latent image) and (ii) simulation of resist developed images at electron and ion beam lithography as well as the peculiarities of the developed Monte Carlo models are described and discussed in these two chapters (part 1 and part 2).

## 2. Deposited energy in the case of electron beam lithography simulation

The first main step of a complete mathematical model for electron beam lithography (EBL) simulation is to simulate the exposure of polymer resist films. During the exposure process the resist material modifies the local solubility rate. The main goal during the exposure process modeling is the calculation of the absorbed energy space distribution. There exist two types of method to calculate the deposited energy in the resist (latent image): analytical methods (Hatzakis et al., 1974; Hawryluk et al., 1974; Raptis et al., 1998) and numerical methods (Kyser & Murata, 1974; Adesida et al., 1979; Vutova & Mladenov, 1994). The analytical method is based on some particular approximations that simplify the nature of the real process (small-angle and diffusion particle scattering, single-component targets, point source or source of homogeneous cross section, etc). These assumptions do not correspond to the real process of the beam scattering within the target. Nevertheless, the

Source: Lithography, Book edited by: Michael Wang,  
ISBN 978-953-307-064-3, pp. 656, February 2010, INTECH, Croatia, downloaded from SCIYO.COM

simulation of energy deposition in the resist film coated on patterned substrates using analytical methods is very difficult if not impossible.

The numerical methods, based on the Monte Carlo (MC) technique for the statistical electron trajectory modeling and energy loss calculation, have been extensively developed and have become the most accepted methods in this field. The MC method mirrors the real process and in the case of large-number trajectory modeling, assures high statistical accuracy and satisfactory consistency. On the other hand, the MC method is ideal for parallel processing computers.

In the proposed simulation model the absorbed energy space distributions are calculated using MC algorithm for electron penetration and energy-loss calculation, which has four sub-steps: (i) forming an electron scattering model and calculating the discrete absorbed energy distribution in the resist film due to a point beam, (ii) approximating the absorbed energy using analytical expressions (energy deposition function EDF( $r,z$ )), (iii) convoluting the function EDF( $r,z$ ) with the actual current distribution in the electron beam used for exposure, (iv) calculating the spatial distribution of the absorbed energy density in the resist which determines the obtained latent image during the electron beam exposure process of the desired layout. The process resolution is limited by the phenomena of forward deflection and backscattering of the electrons during their passage through the resist layer and the substrate. When a real micro-image is exposed, the absorbed energy in every resist volume point can be calculated by summing up the energy losses, obtained in regions far from the beam incident point (several  $\mu\text{m}$ ). In this way the scattering of the beam electrons limits the lateral resolution of the exposed lithographic patterns and patterning of dense high-resolution layouts. This phenomenon is known as a proximity effect and the function EDF( $r,z$ ) characterizes the so-called proximity effect (undesired exposure dose due to backscattered electrons) (Chang, 1975).

Calculation of energy deposition in the resist film due to a point beam (with a zero-width beam diameter  $\delta$ -function) requires to investigate thousands electron trajectories, i.e. millions collisions between accelerated electrons and scattering target atoms (an elementary collision sequence with target atoms). We calculate the characteristic changes in the particle motion for each collision, assuming a straight-line trajectory between two collisions (Fig.1). The scattering atom is presented by a shielded Coulomb potential. The scattering angle  $\theta$  of the penetrating electron is calculated using the differential scattering cross-section for the penetrating electron (for elastic collisions with target atoms) and assuming a Rutherford shielding potential presenting the scattering atom:

$$\frac{d\sigma}{d\Omega} = \frac{e^4}{(2mV^2 4\pi\epsilon_0)^2} \left[ \frac{Z}{\sin^2\left(\frac{\theta}{2}\right) + \beta^2} \right]^2 = \frac{1.3 \cdot 10^{-19}}{E^2} \left[ \frac{Z}{\sin^2\left(\frac{\theta}{2}\right) + \beta^2} \right]^2, \quad (1)$$

where  $\sigma$  is the differential scattering cross section [ $\text{mm}^2$ ],  $\Omega$  is the solid angle,  $V$  is the velocity and  $E$  [eV] is the energy of the penetrating electron,  $Z$  is the atomic number of the scattering atom. The shielding parameter  $\beta$  characterizes the minimal scattering angle at which the value of  $d\sigma/d\Omega$  does not increase more when the value of  $\theta$  decreases:

$$\beta = 2.33 (Z^{1/3}/E^{1/2}) \quad (2)$$

and then the total cross section of the elastic scattering is:

$$\sigma = \frac{0.126 \cdot 10^{-17} Z^2}{E^2 \beta^2 (\beta^2 + 1)}, \tag{3}$$

where  $\sigma$  [m<sup>2</sup>] if E [eV].

The non-elastic scattering weakly changes the electron trajectory due to its domination only at very small values of the scattering angles. It is taken into account as  $Z^2$  is replaced by  $Z(Z+1)$  in Eq.(1) and Eq.(3). The mean energy losses of the penetrating electrons, evaluated per one unit of the trajectory length are:

$$-\left\langle \frac{dE}{d\xi} \right\rangle = \frac{e^4 N_A \rho}{8\pi\epsilon_0^2 E} \sum_i \frac{c_i Z_i}{M_i} \ln\left(1.166 \frac{E}{I_m}\right), \tag{4}$$

where  $dE/d\xi$  [eV/Å], the target density  $\rho$  [g/cm<sup>3</sup>], E [eV],  $N_A$  is the Avogadro's number,  $c_i$  is the weight portion of the i-kind of the target atoms,  $M_i$  is their atomic weight,  $I_m$  is the average ionization potential.

The program involves a MC technique to calculate the kind of the atom taking part in the collision, the azimuthal angle value, ect. The probability for a collision with the target atom of k-kind is:

$$P_k = (n_k \cdot \sigma_k) / \left( \sum_{i=1}^m n_i \cdot \sigma_i \right), \tag{5}$$

where m is the number of the different kinds of the target atoms. The scattering cross-section  $\sigma_i$  is calculated using Eq.(3) for the electron energy E before the collision. The concentration  $n_k$  of this kind of atoms is calculated using:

$$n_k = c_k (\rho / \bar{M}) N_A, \tag{6}$$

where  $\bar{M}$  is the average target molecular weight. The length of the mean free path between two collisions of the penetrating electron is distributed in  $[0, \infty]$  with a probability density:

$$p(\lambda) = \frac{1}{\lambda_0} \exp\left(-\frac{\lambda}{\lambda_0}\right), \tag{7}$$

where  $\lambda_0 = \left( \sum_{i=1}^m n_i \sigma_i \right)^{-1}$ . The distance that the electron travels between these collisions is:

$$\Delta\xi = -\lambda_0 \ln(1-R_1), \tag{8}$$

where  $R_1$  is a random number evenly distributed in  $[0,1]$ . The energy losses of the penetrating electron at the interaction with the target electrons along this path are calculated using the Bethe energy-loss Eq.(4). The scattering angle of the collision is calculated:

$$\cos\theta = 1 - \frac{2\beta_k^2 R_2}{1 + \beta_k^2 - R_2}, \tag{9}$$

The azimuthal angle  $\varphi$  is given by:

$$R_3 = \frac{\phi}{2\pi}, \tag{10}$$

where  $R_2$  and  $R_3$  are also random numbers. Due to the big difference concerning the weights of the particles, the energy losses at the collision between the penetrating electron and scattering atom are neglected. The values of  $\Delta\xi$ ,  $\theta$  and  $\phi$  for each collision are calculated. The calculation is repeated to yield new position in the target for a new set of random numbers until the energy of the electron falls below a predefined value (500 eV) or the electron leaves the target. Then the electron trajectory is calculated (Fig.2).

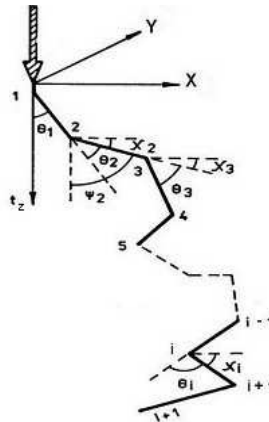


Fig. 1. Geometrical parameters for the electron scattering in the sample.

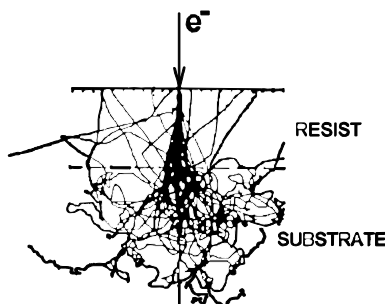


Fig. 2. Simulated trajectories of 100 electrons in PMMA, the electron energy is 30 keV.

The trajectory can be presented in the coordinate system  $Oxyt_z$  (easily connected with a cylindrical system, and  $r = (x^2 + y^2)^{1/2}$ ), where the axis  $t_z$  is parallel to the initial direction of the penetrating electron motion (usually this direction is perpendicular to the target surface) and using the relation:

$$\cos\psi_i = \cos\psi_{i-1} \cdot \cos\theta_i + \sin\psi_{i-1} \cdot \sin\theta_i \cdot \cos\phi_i. \tag{11}$$

The angles  $\psi_{i-1}$ ,  $\psi_i$  and  $\theta_i$  are shown in Fig.1. The angle  $\phi_i$  is the azimuthal angle of scattering for the  $i$ -th collision. The point depth  $t_z$  for the  $(i+1)$ -th collision is calculated using the formula:

$$(t_z)_{i+1} = \sum_{k=1}^i \Delta \xi_k \cos \psi_k = (t_z)_i + \Delta \xi_i \cdot \cos \psi_i. \tag{12}$$

The distance to the coordinate axis  $0t_z$  is calculated by analogy assuming that the angle  $\chi_i$  determines the trajectory path projection on the axis  $Or$ , as well as that the angle  $\phi_i$  corresponds to the azimuthal angle  $\varphi_i$ . The following equations present the relations between these angles:

$$\sin \psi_o = \cos \chi_o \tag{13}$$

$$\cos \psi_o = \sin \chi_o \tag{14}$$

$$\phi_i = \varphi_i - \arccos \frac{-\cos \psi_{i-1} \cdot \cos \chi_{i-1}}{\sin \psi_{i-1} \cdot \sin \chi_{i-1}} \tag{15}$$

$$\cos \chi_i = \cos \chi_{i-1} \cdot \cos \theta_i + \sin \chi_{i-1} \cdot \sin \theta_i \cdot \cos \phi_i \tag{16}$$

$$\sin \chi_i = \sqrt{1 - \cos^2 \chi_i}. \tag{17}$$

Then:

$$r_{i+1} = \sum_{k=1}^i \Delta \xi_k \cos \chi_k = r_i + \Delta \xi_i \cos \chi_i. \tag{18}$$

The energy losses for each segment (a straight line trajectory between two collisions) of the free path  $\Delta \xi_i$ , is represented as  $\left\langle \frac{dE}{d\xi} \right\rangle \cdot \Delta \xi_i$  and can be assumed as the energy losses in the point of the  $i$ -th collision for the corresponding elemental volume in the target. We check the energy of the electron and its position in the target. The calculation for this particle stops if the energy falls below the minimal predefined value (500 eV) or the electron leaves the sample. Then the calculation for new electron starts. After summing up the losses corresponding to the all  $N$  penetrating electrons, we obtain discrete data (a two-dimensional data array) for a radial energy deposition function (EDF) at various resist depths from the point of beam incidence. It is possible to use various cell dimensions at different radial distances: lower values near the point of beam incidence and higher values far away from this point. When using a Cartesian coordinate system instead of a cylindrical one it is possible to simulate beam incidence inclined to the resist surface (Gueorguiev, 1996). There are procedures for re-calculation of the free path and electron stopping power when a penetrating electron crosses the interfaces in multilayer structures (Gueorguiev et al., 1994). To achieve a satisfactory statistical accuracy, using MC calculations, a large number of particle trajectories are simulated ( $10\text{-}20 \times 10^3$ ). A detailed description and obtained results are presented in (Vutova & Mladenov, 1994; Mladenov & Vutova, 2002; Vutova, 2007).

**2.1 Results and discussion**

We have developed a program which realizes the MC algorithm to model the electron scattering in multilevel multicomponent amorphous targets, named TREM-MV. Using the simulation tool, calculations over a wide range of primary electron beam energies and resist

thickness values are performed for different substrates (Vutova & Mladenov, 1994; Gueorguiev et al., 1995; Mladenov & Vutova, 2002; Vutova et al., 2007). In Fig.2 calculated trajectories in the case of a 1  $\mu\text{m}$  thick poly-methyl methacrylate (PMMA) (a widely used polymer resist) on Si substrate are shown. The chemical composition of this resist is  $\text{C}_5\text{H}_8\text{O}_2$ , the efficient atomic number is  $Z=3.6$ , the atomic mass is  $M = 6.7$  and the polymer density is  $\rho = 1.22 \text{ g/cm}^3$ .

Fig.3 presents the radial distribution of the electron energy deposition in the resist film for 0.12  $\mu\text{m}$  thick PMMA on Si due to a point beam by tracing 10 000 electron trajectories (for each simulation). Two characteristic regions can be seen: a narrow one, near the beam axis, with an abrupt drop, which represents the forward scattering electron contribution to the function  $\text{EDF}(r,z)$  and a wide part with a slightly varying drop, which corresponds to the backscattering electron contribution. As the initial electron energy increases, the area of the forward scattering electrons broadens insignificantly, while the region of the backward scattering electrons undergoes considerable broadening.

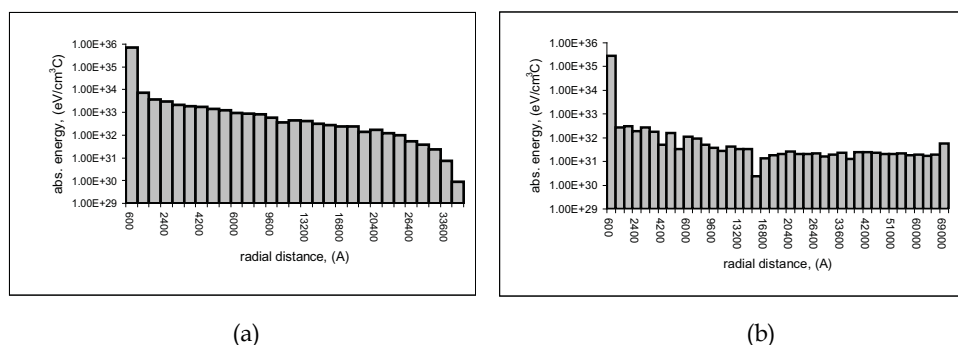


Fig. 3. (a) - 0.12  $\mu\text{m}$  PMMA/Si,  $E_0 = 20 \text{ keV}$ , (b) - 0.12  $\mu\text{m}$  PMMA/Si,  $E_0 = 50 \text{ keV}$

Another presentation of the calculation results is by means of the equi-energy density contours as shown in Fig.4. When increasing the polymer thickness (Fig. 4(a)-(c)) a deviation of the most distant equi-energy density contours from the beam axis is observed, which is due to broadening of the forward scattering electron area. Further increase of the resist thickness (Fig.4(d)) results in a deviation of the equi-energy density contours back to the beam axis which is due to the beam intensity decrease. The doses corresponding to the presented equi-energy density contours decrease starting from the beam axis as follows: 1; 1/2; 1/4; 1/10; 1/20; 1/75. These results can be used both for the latent image profile prediction under particular exposure conditions and for the exposure condition optimization, allowing the desired profile to be obtained. For example, one can see from Fig.4, that to obtain a latent image with vertical walls (primary e-beam energy, 20 keV) it is preferable to use thin polymer film whose thickness is less than 0.4  $\mu\text{m}$ .

The high resolution of EBL however may be degraded by the lateral scattering of incident electrons which causes undesired exposure of unintended regions of the resist. This phenomenon is commonly referred to as proximity effect. In the case of patterning the thin films of the most widely used high temperature superconducting (HTS) material, namely  $\text{YBa}_2\text{Cu}_3\text{O}_{7-\delta}$  (YBCO) deposited on  $\text{SrTiO}_3$  (STO),  $\text{MgO}$ ,  $\text{ZrO}_2$ ,  $\text{Y}_2\text{O}_3$ ,  $\text{LaAlO}_3$ ,  $\text{NdGaO}_3$ , etc. substrates an enhanced proximity effect has to be taken into account because of their

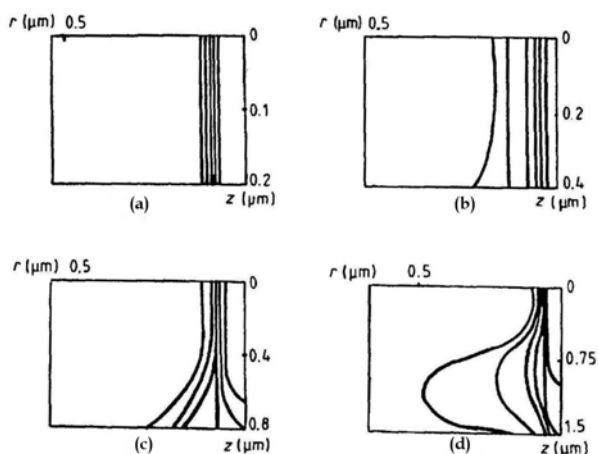


Fig. 4. The calculated equi-energy density contours in a 0.2, 0.4, 0.8 and 1.5  $\mu\text{m}$  PMMA film on Si generated by an electron beam of 20 keV.

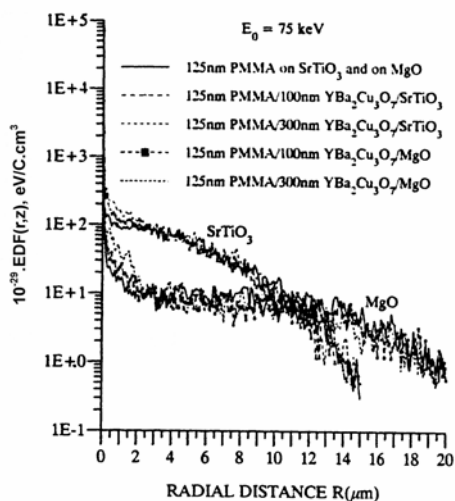


Fig. 5. Radial distributions of the absorbed energy density in the resist at  $E_0 = 75$  keV.

retively high effective atomic numbers (Gueorguiev, 1994). Using our program for MC simulation of the processes of penetration and scattering of accelerated electrons in solids, the radial distributions of the EDF in 125 nm PMMA resist layer coated on structures YBCO thin film/substrate are obtained for an e-beam in the form of a zero-width  $\delta$  function, 30 000 electron trajectories, and the following parameters: (i) the substrate material (STO and MgO), (ii) the e-beam energy  $E_0$  (25, 50 and 75 keV), and (iii) the YBCO film thickness  $d$  (0, 100, and 300 nm). In Fig.5, the calculated radial distributions of the absorbed electron energy density at  $E_0 = 75$  keV are shown as an example. The results show that the EBL on the above mentioned targets is associated with an enhanced proximity effect in comparison with that

on the conventional in microelectronics targets PMMA/Si substrate or PMMA/SiO/Si substrate. Moreover, the HTS thin film causes an additional backscattering of penetrating electrons and, hence, an additional proximity effect (in comparison with the targets PMMA/STO and PMMA/MgO) in the regions close to the incident point of the electron beam. This effect is as greater, as thicker is the film, as lighter is the substrate, as lower is the beam energy and is not completely eliminated even at energies as high as 75 keV, especially for the film thickness 300 nm, as well as for the lighter substrate (MgO).

### 3. Approximation of the discrete data for the deposited energy in the resist using analytical functions

Due to large lateral scattering of the penetrating electrons, the exposure of many image segments effects the total deposited energy in a specific resist point. This effect, known as a proximity effect, requires high accuracy evaluation of the EDF at large radial distances i.e. far away from the point of incidence. It should be pointed out that the increase of the number of trajectories being modeled, with the purpose of achieving statistical consistency for large lateral distances (characterizing the backward scattered electrons and giving the greatest contribution to the proximity effect) is not quite effective, as only a few trajectories travel through these regions. A MC methodology and a corresponding computer program BET-MK are developed for transformation of the numerical data array, representing the absorbed energy space distribution when exposing one point from the resist surface, into the form of analytical functions (Vutova & Mladenov, 1994). In this way the problem concerning the insufficient statistics of the discrete data for the absorbed energy in the case of large lateral distances is overcome. The main features of this methodology are as follows:

- i. Transformation of numerical data for the absorbed energy discrete space distribution in the form of analytical functions. The data arrays containing the energy distribution when exposing one point from the resist surface are obtained using the TREM-MV program.
- ii. The absorbed energy at some resist depth in the case of Si substrate is approximated as a sum of two Gaussians:

$$f(r) = k[\exp(-\frac{r^2}{\delta_f^2}) + \eta_E \cdot \frac{\delta_f^2}{\delta_b^2} \cdot \exp(-\frac{r^2}{\delta_b^2})] \quad (19)$$

where  $k$  is a normalization constant,  $\delta_f$  and  $\delta_b$  are the characteristic widths of the forward and the backward scattering particles, and  $\eta_E$  is the ratio of the energy depth dissipation of the backward scattering particles to that of the forward scattering particles. The input data for the program BET-MK is the 2-D arrays EDF( $r,z$ ) containing the absorbed energy distribution values obtained as a result of the trajectory modeling. The first Gaussian (with standard deviation  $\delta_f$ ) dominates for the short lateral distances and describes the energy deposition from the forward scattered electrons. The second Gaussian (with standard deviation  $\delta_b$ ) dominates for the long lateral distances and describes the contribution from the backscattered electrons. The parameters  $\delta_f$ ,  $\delta_b$  and  $\eta_E$  are called proximity effect parameters.

- iii. The parameter values ( $\delta_f$ ,  $\delta_b$ ,  $\eta_E$ ) are calculated using an original MC technique, instead of the non-linear least-square method and an arbitrary kind of distribution. The

technique comprises the mean square deviation minimization by the interval length decrement for each of the parameters chosen. The minimization is made in an iteration loop.

The main advantages of the MC technique described above are: (i) in contrast to some of the least-squares methods, it does not allow the possibility of an infinite loop in the case of a local minimum; (ii) it enables to approximate an arbitrary kind of distribution of numerical data with a corresponding analytical function.

Fig.6 presents the EDF in the resist film for 0.4  $\mu\text{m}$  thick PMMA on Si for 50 keV beam energy. The standard deviation for forward ( $\delta_f$ ) and backscattering ( $\delta_b$ ) contributions (Eq.19) as calculated from the simulation data are:  $\delta_f = 0.165 \mu\text{m}$ ,  $\delta_b = 7.769 \mu\text{m}$ ,  $\eta_E = 1.2$ .

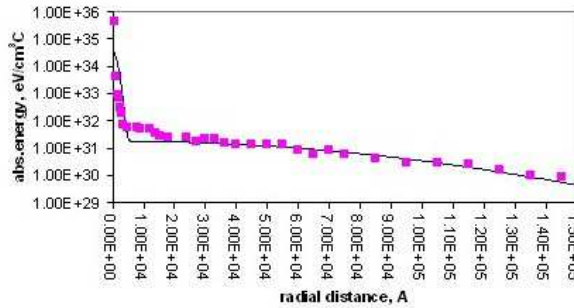


Fig. 6. Comparison between the deposited energy distribution (EDF) in the case of PMMA on Si at the interface resist/silicon and the corresponding analytical fit (Eq.19). The electron beam is focused on a surface point. The symbols (•) present the results for MC calculation (TREM-MV), the line (-) for  $f(x)$ .

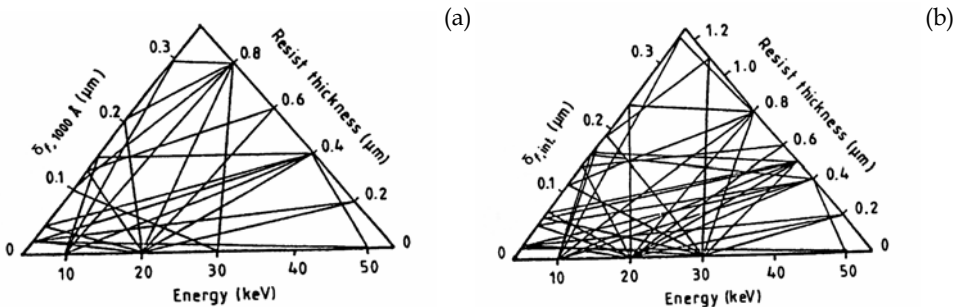


Fig. 7. Dependence of  $\delta_f$  on incident electron energy and on resist (PMMA) thickness at two characteristic depths: (a) resist surface (1000 Å in depth); (b) film-substrate interface.

The values of the parameters  $\delta_f$  and  $\delta_b$  for various electron beam energies and different resist (PMMA) thicknesses are shown in Figs.7-8. In the triangular diagram the points corresponding to the values of  $\delta_f$  or  $\delta_b$ , the resist depth, and the beam energy represent vertices of inscribed triangles. Using these results one can approximate determine the  $\delta_f$  and  $\delta_b$  values for different beam energies and resist thicknesses. For instance, if the beam energy is 15 keV and the PMMA thickness is 0.8  $\mu\text{m}$ , the  $\delta_f$  value at the depth of 0.1  $\mu\text{m}$  is in the range of [0.21, 0.29]  $\mu\text{m}$ , and that at the resist-substrate interface is between 0.24 and 0.33  $\mu\text{m}$ . If the

beam energy is 20 keV, the PMMA thickness is 0.7 μm, the δ<sub>b</sub> value at the depth of 0.1 μm is in the range of [0.13, 0.21] μm, and at the resist-substrate interface its value is between 0.14 and 0.23 μm. Similarly, if δ<sub>f</sub> (or δ<sub>b</sub>) values and the beam energy are known, one can determine the resist thickness and vice versa from known δ<sub>f</sub> (or δ<sub>b</sub>) and the resist thickness, the beam energy can be determined.

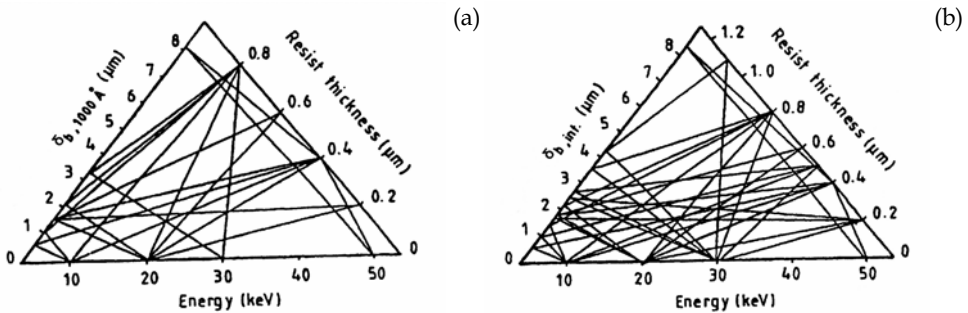


Fig. 8. Dependence of δ<sub>b</sub> on incident electron energy and on resist (PMMA) thickness at two characteristic depths: (a) resist surface (1000 Å in depth); (b) film-substrate interface.

According to the simulation strategy, the next step in the modeling is the convolution of EDF(*r,z*) with the actual beam current distribution *j*(*r,z*), giving the single-energy deposition function (SEDF(*r,z*)). Let the electron beam is Gaussian distributed with a characteristic width δ\*, i.e.

$$j = j_0 \cdot \exp\left(-\frac{r^2}{\delta^{*2}}\right) = \frac{I_b}{\pi \cdot \delta^{*2}} \exp\left(-\frac{r^2}{\delta^{*2}}\right), \tag{20}$$

where *I<sub>b</sub>* is the incident beam current, *j* and *j<sub>0</sub>* are the current densities at a distance *r* and at the beam centre, respectively. Then the function for a real e-beam can be calculated by the convolution of (19) and (20). The result from this convolution is the function *f*<sup>\*</sup>(*r*), that has an analytical representation in the form of (19), but its characteristic widths are now modified:

$$\delta_f^* = (\delta_f^2 + \delta^{*2})^{1/2} \tag{21}$$

$$\delta_b^* = (\delta_b^2 + \delta^{*2})^{1/2}. \tag{22}$$

#### 4. A three-dimensional model for absorbed energy calculation

To obtain the absorbed energy space distribution when exposing an arbitrary pattern, using an arbitrary exposure dose distribution, one must take into account the influence of a large number of exposed points. This is due to the fact that the lithography micro-patterning includes many irradiated points. Integrating the data obtained by the computer simulation of the exposure of each point from the resist surface, the absorbed energy space distribution in the case of an arbitrary pattern can be calculated. Due to the large number of calculations, a simplified procedure should be used to calculate the integral space distribution of the absorbed energy. The main features of the procedure proposed in (Vutova & Mladenov, 1991) are as follows.

- i. The two-dimensional data array containing the absorbed energy values at some resist depth is presented as (19). If the electron (or ion) exposure is uniformly distributed over an area  $A$ , then the energy density can be expressed as:

$$F(r) = \oint_A f^*(r).dA \tag{23}$$

If the area  $A$  is a simple pattern (i.e. a line or a rectangle) the integral (23) can be calculated using the tabulated error function:

$$\text{erf}(t,\sigma) = \int_0^t \exp(-\frac{x^2}{\sigma^2}).dx \cdot \tag{24}$$

- ii. In the case of a more complex pattern, it should be divided into simple parts and then the corresponding values of the absorbed energy should be subsequently summed up. The formulas obtained for the absorbed energy density, when exposing either a line, a line segment, or a rectangle (Vutova & Mladenov, 1991), are given below. These simple patterns are sufficient to compose an arbitrary figure.
- iii. The procedure takes into account the radial variation of the absorbed energy as well as its modification versus the depth of the resist. To calculate the  $\delta_f$ ,  $\delta_b$ , and  $\eta_E$  parameter values, the linear approximation along the resist depth is used. In the electron exposure case, two resist depths are used, namely the resist surface and the resist-substrate interface (Table 1). The proposed methodology is realized in a computer program.

Beam energy [keV]	Resist thickness [ $\mu\text{m}$ ]	Resist depth [ $\mu\text{m}$ ]	$\delta_f$ [ $\mu\text{m}$ ]	$\delta_b$ [ $\mu\text{m}$ ]	$\eta_E$
50	0.4	0.1	0.145	6.67	1.19
50	0.4	0.2	0.152	7.036	1.19
50	0.4	0.3	0.1583	7.403	1.194
50	0.4	0.4	0.165	7.77	1.2
20	0.4	0.1	0.0412	1.51	0.75
20	0.4	0.2	0.0434	1.53	0.759
20	0.4	0.3	0.0458	1.575	0.763
20	0.4	0.4	0.049	1.652	0.768
20	0.8	0.1	0.203	2.08	0.485
20	0.8	0.3	0.206	2.11	0.485
20	0.8	0.5	0.221	2.13	0.497
20	0.8	0.7	0.228	2.13	0.503
20	0.8	0.8	0.235	2.17	0.503

Table 1. Proximity effect parameters (Eq.19) obtained by means of program TREM-MV and BET-MK for a point source.

Let we have Cartesian coordinate system  $Oxyz$ , such that the axis  $Ox$  and  $Oy$  are in the plane of the resist surface, the axis  $Oz$  is in its depth, and  $x^2 + y^2 = r^2$ . Let we expose a line segment and the axis  $Oy$  coincides with the line segment, whose end points are labeled  $a$  and  $b$  (Fig.9).

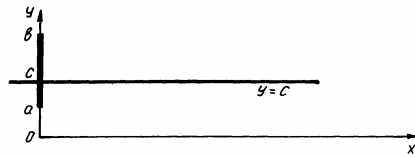


Fig. 9. A case of the exposed segment (the single isolated line of finite length).

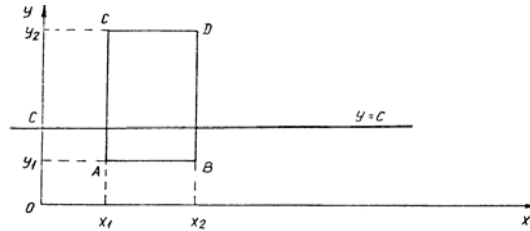


Fig. 10. A case of the exposed rectangle.

We are interested in the cross section that is perpendicular to the segment line and whose analytical expression is  $y = c$ . From (19) and (23) we obtain:

$$F(r) = \int_a^b f^*(r)dy = (b - a)f(r) = (b - a)k[\exp(-\frac{x^2 + c^2}{\delta_f^2}) + \eta_E \frac{\delta_f^2}{\delta_b^2} \exp(-\frac{x^2 + c^2}{\delta_b^2})]. \tag{25}$$

Similarly, we can obtain the expressions for the density of the absorbed energy in a point lying at the  $y = c$  line, when exposing a rectangle ABCD (Fig.10):

a. for  $x < x_1 < x_2$

$$F(r) = (y_2 - y_1)k\{\exp(-\frac{c^2}{\delta_f^2})[erf(x_2 - x, \delta_f) - erf(x_1 - x, \delta_f)] + \eta_E \frac{\delta_f^2}{\delta_b^2} \exp(-\frac{c^2}{\delta_b^2})[erf(x_2 - x, \delta_b) - erf(x_1 - x, \delta_b)]\} \tag{26}$$

b. for  $x_1 \leq x \leq x_2$

$$F(r) = (y_2 - y_1)k\{\exp(-\frac{c^2}{\delta_f^2})[erf(x_2 - x, \delta_f) + erf(x - x_1, \delta_f)] + \eta_E \frac{\delta_f^2}{\delta_b^2} \exp(-\frac{c^2}{\delta_b^2})[erf(x_2 - x, \delta_b) + erf(x - x_1, \delta_b)]\} \tag{27}$$

c. for  $x_2 < x$

$$F(r) = (y_2 - y_1)k\{\exp(-\frac{c^2}{\delta_f^2})[erf(x - x_1, \delta_f) - erf(x - x_2, \delta_f)] + \eta_E \frac{\delta_f^2}{\delta_b^2} \exp(-\frac{c^2}{\delta_b^2})[erf(x - x_1, \delta_b) - erf(x - x_2, \delta_b)]\} \tag{28}$$

where  $erf(t, \sigma)$  is calculated using (24).

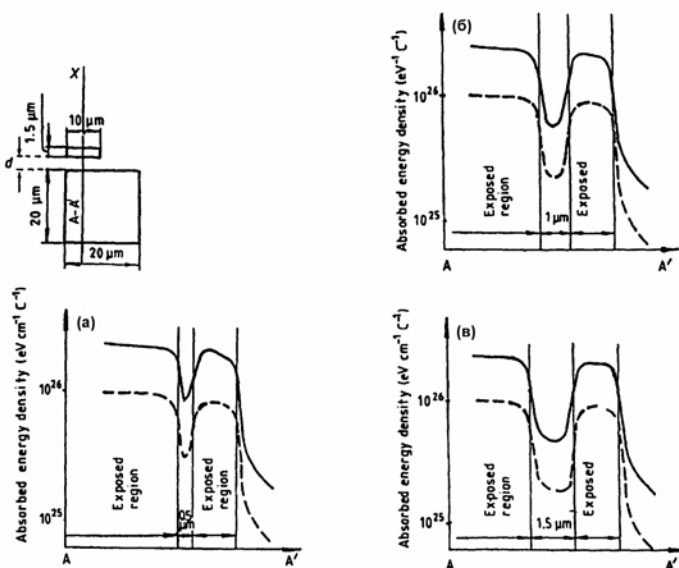


Fig. 11. Variation of the EDF along the line A-A' at the top layer (1000 Å in depth, broken curves), and at the bottom of the resist (8000 Å, full curves), for a 0.8 μm PMMA on Si for a 20 keV Gaussian e-beam. Inter-element spacings are (a) 0.5 μm, (b) 1.0 μm, and (c) 1.5 μm.

The absorbed energy density distribution in the case of a more complex topological structure, where the proximity effect cannot be ignored is shown in Fig.11. The results are presented for three inter-elemental spacings of  $d=0.5, 1.0,$  and  $1.5 \mu\text{m}$ . This simulation result clarifies the effects of an adjacent element and its configuration on the energy distribution.

### 5. Absorbed energy approximation in the case of multilayers samples and heavy substrates

The proximity effect in the case of patterning the thin films of the most widely used HTS material, namely YBCO, deposited on two typical substrates (STO and MgO) is investigated (Gueorguiev et al., 1995; Gueorguiev et al., 1996; Gueorguiev et al., 1998; Olziersky et al., 2004; Vutova, 2007). HTS samples represent a more difficult case study since the substrate consists of bulk substrate STO or MgO and a very thin YBCO layer on top (multilayer substrate). The existence of the thin YBCO film between the bulk substrate and the resist changes the scattering phenomena and has to be carefully taken into account. This effect becomes more important as film thickness increases.

For substrates with larger mean atomic number and density the addition of one more function is necessary. In the case of YBCO films over STO or MgO substrates the addition of an exponential function in equation (19) is found to be adequate (Gueorguiev et al., 1996). Thus EDF( $r$ ) could be approximated as:

$$f(r) = \frac{k}{\pi(1+\eta+\nu)} \left[ \frac{1}{\alpha^2} \exp\left(-\frac{r^2}{\alpha^2}\right) + \frac{\eta}{\beta^2} \exp\left(-\frac{r^2}{\beta^2}\right) + \frac{\nu}{2\gamma^2} \exp\left(-\frac{r}{\gamma}\right) \right], \quad (29)$$

where the third term describes the energy deposition in the mid-lateral distances. The values of the parameters of this function (called proximity function)  $a$ ,  $\beta$ ,  $\gamma$ ,  $\eta$ ,  $\nu$  and  $k$  are calculated using the MC technique (described above 3.).

### 5.1 Results and discussion

The variables studied in our work are the substrate material (STO and MO), the initial energy of accelerated electrons  $E_0$  (25, 50 and 75 keV) and the HTS film thickness  $d$  (0, 100, 200, 300 and 1000 nm). The values of the proximity effect parameters are evaluated from the fitting of EDF( $r$ ) with a sum of suitable functions (Eq.29) and their dependence on all investigated variables are discussed (Gueorguiev et al., 1995; Gueorguiev et al., 1996; Gueorguiev et al., 1998; Olziersky et al., 2004). The absorbed energy distributions obtained and the calculated parameters of the proximity function can be used in a proper proximity effect correction algorithm as well as in a resist profile development model. The proximity effects are usually compensated for by applying proper correction algorithms which adjust the exposure dose and/or the shape and size of the exposed pattern. For the realization of such algorithms precise data are required about the spatial distribution of absorbed electron energy density in the resist. This distribution quantitatively describes the proximity effects.

In Fig.12 a comparison is made between the radial distributions of the absorbed energy density obtained by MC simulation for the structure 125 nm PMMA resist film /300 nm YBCO HTS film /MgO substrate at three beam energies -25, 50, and 75 keV, and the corresponding analytical fits. It is well seen that the combination of double Gaussian and exponential functions is a good approximation of these distributions. Although not shown here, the double Gaussian (Eq.19), as well as the triple Gaussian were also tested but they were found to be not adequate, especially in the intermediate regions (Fig.12).

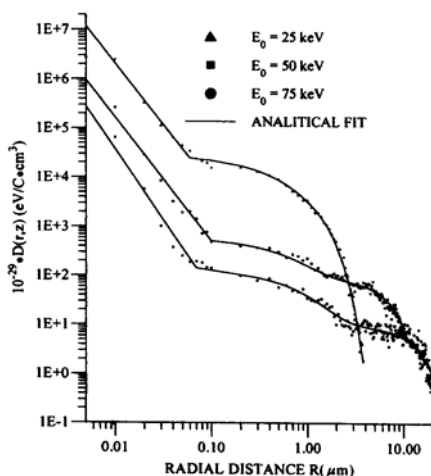


Fig. 12. Comparison between the exposure distributions obtained by MC simulation for the structure 125 nm PMMA resist film / 300 nm YBCO HTS film / MgO substrate at three beam energies - 25, 50, and 75 keV and the corresponding analytical fits.

Figure 13 shows the analytical fit to the radial distributions of absorbed energy density obtained by MC simulation for the structures 125 nm PMMA resist film /0, 100, or 300 nm

YBCO HTS films / STO or MgO substrates at 25, 50, and 75 keV, respectively. Since the aim is to investigate the proximity effects caused by YBCO film as well as by the substrate (STO, MgO) the backscattered exposure is of primary importance. For this reason here, in contrast to the Fig.12, a linear scale for the  $x$  axis is applied which although it compresses data points close to the beam axis (associated with the forward scattered electrons), it ensures a better distinction between the distributions in their intermediate and distant regions (associated with backscattered electrons).

The peaks of the distributions of the absorbed energy density are commonly attributed to the forward scattering of electrons or, in other words, to the single scattering of primary electrons into small angles in the resist. This scattering depends on the beam energy as well as on the material and thickness of the resist. In Figs.12-13 it is seen that the maximum values as well as the widths of the peaks decrease with increasing beam energy. This can be explained by both the more efficient scattering of primary electrons and the higher energy loss in the resist at lower energies.

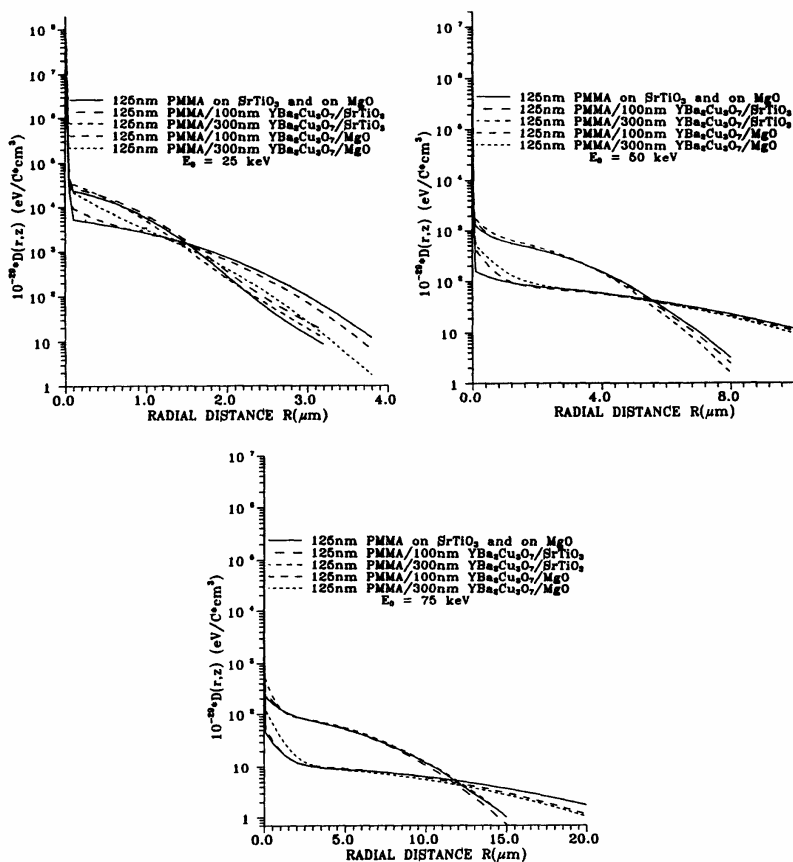


Fig. 13. Analytical fit of the exposure distributions in a 125 nm PMMA resist film on STO and MO substrates as well as on 100 and 300 nm HTS layers of YBCO deposited on the substrates,  $E_0=25, 50, 75$  keV.

The calculated values of the parameters of the analytical function and their dependencies on the beam energy and on HTS film thickness are presented in the form of triangular diagrams as well as of 3D diagrams that can be used for easy approximate determination of the parameters at different beam energies and YBCO film thicknesses – Fig.14 and Fig.15.

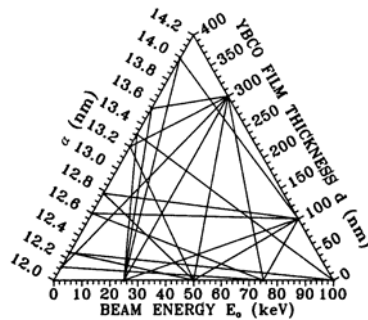


Fig. 14. Dependence of the parameter  $\alpha$  of the proximity function on YBCO film thickness  $d$  and the beam energy  $E_0$  for STO substrate.

The results show that the additional backscattering of primary electrons and, hence, the proximity effect, caused by the HTS film in the regions close to the incident point of the electron beam are not completely eliminated even at energies as high as 75 keV especially for the film thickness 300 nm as well as for the lighter substrate (MgO). The HTS thin film reduces the backscattering from the underlying substrate and this reduction is as greater as thicker is the film as well as lower is the beam energy.

In Fig.16, EDF( $r$ ) simulation results with the MC method in the case of YBCO/MgO substrates are presented. It is obvious that as  $d_{\text{YBCO}}$  increases, the overall energy deposition approaches the bulk YBCO case. When the YBCO layer is thin, due to its relatively higher scattering parameters (density, mean atomic weight, mean atomic number) in comparison with those for the MgO substrate, the EDF( $r$ ) extends to regions far away from the point of incidence. On the other hand, when the YBCO layer is thick, the backscattered electrons come mainly from this layer rather than the MgO substrate. The external proximity effect obtained in regions far from the point of beam incidence (more than 4–5  $\mu\text{m}$ ) increases

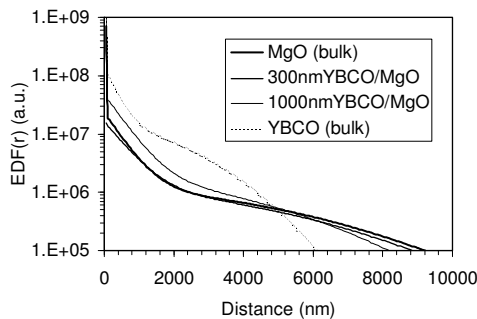


Fig. 16. EDF( $r$ ) simulations for various YBCO thicknesses over MgO bulk substrate using 50 keV e-beam energy.

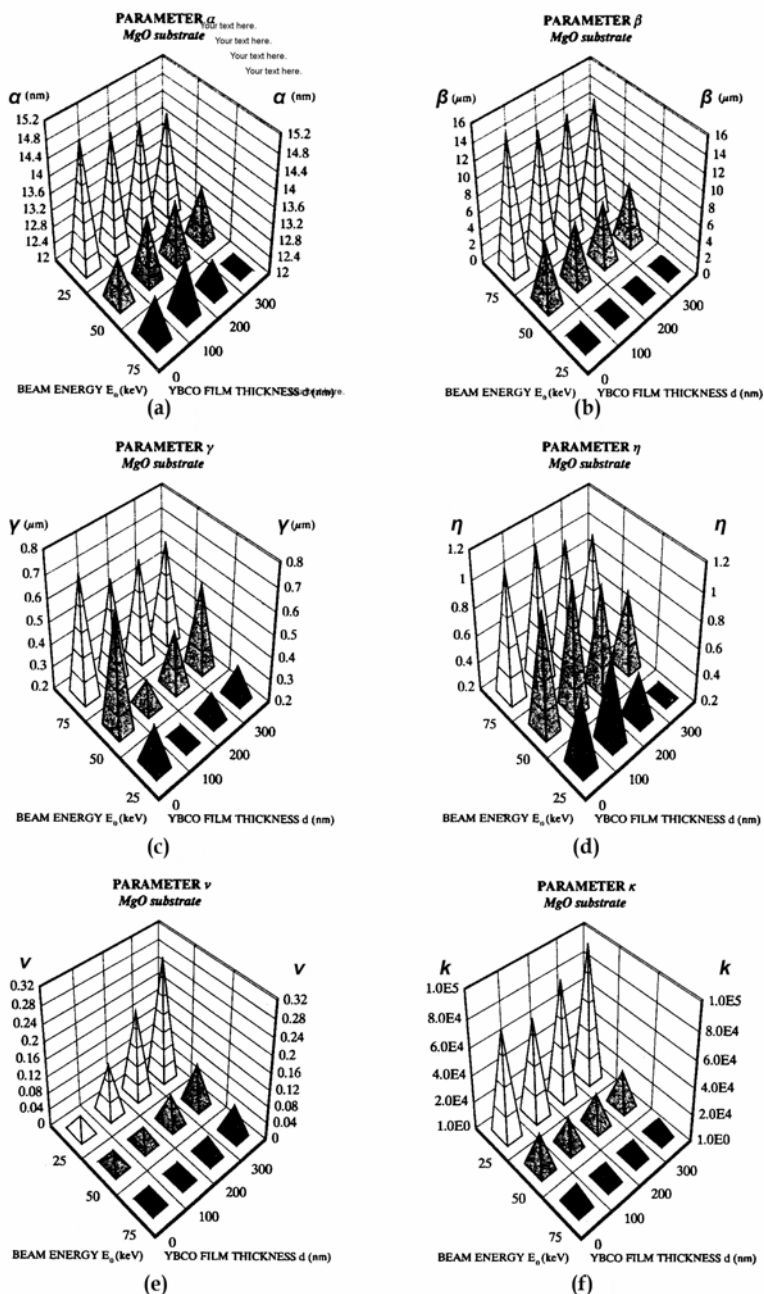


Fig. 15. Diagrams of the dependences of the parameters of the proximity function on the beam energy and YBCO film thickness for the MgO substrate: (a)  $\alpha$ ; (b)  $\beta$ ; (c)  $\gamma$ ; (d)  $\eta$ ; (e)  $\nu$  and (f)  $\kappa$ .

## Thank You for previewing this eBook

You can read the full version of this eBook in different formats:

- HTML (Free /Available to everyone)
- PDF / TXT (Available to V.I.P. members. Free Standard members can access up to 5 PDF/TXT eBooks per month each month)
- Epub & Mobipocket (Exclusive to V.I.P. members)

To download this full book, simply select the format you desire below

